Nanoimprint-Induced Molecular Stacking and Pattern Stabilization in a Solution-Processed Subphthalocyanine Film

Xiaogan Liang,* Teresa Chen, Yeon-Sik Jung, Yoshikazu Miyamoto, Gang Han, Stefano Cabrini, Biwu Ma,* and Deirdre L. Olynick*

The Molecular Foundry, Lawrence Berkeley National Laboratory, 1 Cyclotron Road, Berkeley, California 94720

ABSTRACT We present a systematic study on the thermal nanoimprinting of a boron subphthalocynamine molecule, 2-allylphenoxy-(subphthalocyaninato)boron(III) (SubPc-A), which represents a class of attractive small-molecular weight organic compounds for organic-based photovoltaics (OPV). The final equilibrium imprinted feature profile strongly depends on the imprinting temperature. The highest feature aspect ratio (or contrast) occurs at a specific window of imprinting temperatures (80−90 °C). X-ray diffraction indicates that the nanoimprint at such a temperature window can induce high-degree molecular stacking, which can help stabilize the imprinted features. Outside this window, we observed a pronounced relaxation of imprinted features after template removal, which is attributed to the surface diffusion. Key factors affecting the final equilibrium profile of the imprinted features were simulated. From the simulation, it was found that the crystallization-induced anisotropy of surface energy stabilized imprinted features. Simulated parameters such as stable feature aspect ratio and pitch agree well with experimental data. Such work provides an important guideline for optimizing the nanopatterning of small-molecular-weight organic compounds.

KEYWORDS: nanofabrication · nanoimprint · photovoltaics · subphthalocyanine · surface diffusion

Organic-based photovoltaic cells (OPVs) are of great interest owing to their potential for low-cost solar energy conversion.[1] An important breakthrough for OPVs was the use of a heterojunction (HJ) structure, in which the difference of the energy levels of two materials (donor and acceptor) can lead to efficient dissociation of photogenerated excitons at the HJ interfaces.[1] Since then, tremendous efforts have been taken to optimize the carrier donor/acceptor (DA) interface morphology to improve the photogenerated exciton dissociation and consequently the overall power conversion efficiency.[2] One successful approach is to use a bulk heterojunction (BHJ) structure that can create dissociation centers everywhere within the active layer.[2] Typically, the formation of a BHJ structure can be achieved *via* self-assembly of nanostructured soft materials by spontaneous phase separation in a number of solution processed polymer/fullerene systems, yet efficiency in these structures might be significantly reduced through unpredicted shunt paths and isolated islands of materials.[3] Nanoimprint lithography (NIL) offers a potential solution for producing well-defined interpenetrating networks at the DA interface and is compatible with roll-to-roll manufacturing for low-cost and high-throughput nanopatterning.[4,5] To efficiently harvest photogenerated excitons, densely packed nanoimprinted OPV structures with half-pitch smaller than 2 times that of the exciton diffusion length are needed (typically sub-20 nm regime).[6] Recent efforts in this field have been mainly focusing on polymeric PV materials. However, OPVs with small-molecular weight materials could also benefit from similar morphologies. In addition, small-molecular weight OPV materials provide additional advantages over polymers, such as higher chemical/thermal stability and higher material purity.[7] Previous work has shown relatively poor stability of imprinted nanostructures in small-molecular compounds.[8−10] Problems arise due to pronounced surface diffusion and self-faceting and are exacerbated when features head toward the sub-20 nm regime.[11,12] These instabilities must be understood and overcome to achieve efficient nanostructured OPVs.

Boron subphthalocyanines (SubPcs) are a class of photoactive small-molecular-weight materials with unique physical properties.[13] A typical SubPc has a nonplanar pyramid-shaped structure, in which the boron atom is surrounded by three coupled

*Address correspondence to xliang@lbl.gov, BWMa@lbl.gov, dlolynick@lbl.gov.

Received for review January 13, 2010 and accepted April 16, 2010.

Published online April 22, 2010. 10.1021/nn100075t

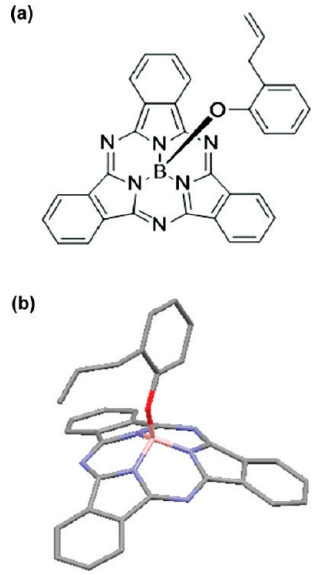

Figure 1. Chemical structure (a) and 3D representation (b) of 2-allylphenoxy-(subphthalocyaninato) boron(III) (SubPc-A).

benzo-isoindole units to give a 14-π-electron aromatic macrocycle (Figure 1). This unique cone-shaped geometry affords SubPcs distinctive physical properties, such as relatively high solubility and low aggregation tendency. Their reasonably broad visible light absorption along with high extinction coefficients of *ca.* 5×10^4 M^{-1} cm^{-1} makes them of great interest as donor materials for OPVs.[14,15] Specifically, for SubPc-A, the incorporation of 2-allylphenoxyl group significantly improves the solubility, allowing the formation of uniform, grain-boundary-free amorphous photovoltaic films *via* simple solution casting. Nanostructuring of the interfaces *via* nanoimprint is expected to significantly improve device performance with these materials. In this work, we systematically investigate the stability of thermally imprinted SubPc-A nanostructures. The final feature aspect ratio (or contrast) strongly depends on the imprinting temperature. The highest final feature contrast is produced by the imprinting at temperatures of 80−90 °C. This coincides with the appearance of clear X-ray diffraction (XRD) peaks associated with the molecular stacking in SubPc-A. Outside of this window, we found that imprinted nanostructures quickly relax to a flat or lower contrast profile after the room-temperature separation of the template from the imprinted SubPc-A layer. This relaxation is driven by the reduction of surface energy. A simulation model was developed to relate nanoimprint-induced molecular stacking with the final equilibrium feature profile. Additional experiments were performed to verify the model.

RESULTS AND DISCUSSION

Figure 2a shows the tilted scanning electron micrograph (SEM) of a nanoimprint template bearing hexagonally arranged posts with a diameter of 20 nm and a feature height of ~22 nm. During an imprinting process at the appropriate range of temperature (55−170 °C) and pressure (1.4−5.5 MPa), SubPc-A can be molded conformably to the template as shown in Figure 2b (imprinting pressure, 3.4 MPa; imprinting temperature, 120 °C) which shows a representative cross-sectional SEM of the template and the molded materials before separation. To further verify that the SubPc-A layer is really conformal to the recesses of a template, we intentionally removed the flat substrate from the SubPc-A without separating the template. This can be achieved by pretreating the Si substrate with a commercial siloxane-based mold release agent, which can significantly reduce the bonding strength between the SubPc-A and the substrate.[16] Afterward, the SubPc-A layer was briefly etched back in O_2 plasma to partially expose the template features (see Figure 2c). Figure 2c clearly demonstrates that the SubPc-A layer is fully conformal to the template features before the template separation. However, after room-temperature separation of this template from the substrate, the imprinted features relax back to an almost flat surface. Figure 3 displays a series of tilted SEM images of the SubPc-A layers imprinted and released using the same template as in Figure 2b (3.4 MPa imprinting pressure, 10 min at imprinting temperatures) but at a range of imprint temperatures. Figure 4 shows the imprinted feature depth as a function of imprinting temperatures for the corresponding template and a larger feature template for comparison. This relaxation of the imprinted features is temperature dependent, and imprinted features are stable only when imprinted within a specific temperature window. For a relatively lower imprinting temperature ($T < 80$ °C), the imprinted hole features exhibit a very shallow aspect ratio and much smaller diameter in comparison with the original template features, which is attributed to the surface relaxation. Between 80 to 90 °C, the imprinting process is effective and the holes have a higher aspect ratio. However, upon further increasing the imprinting temperature ($T > 90$ °C,) the feature aspect ratio is reduced. Figure 4a shows that for the given imprinting conditions, the temperature window for creating the highest feature aspect ratio (or contrast) in the SubPc-A is 80−90 °C. We also compared the imprinting results under two cooling speeds (5 degree/min and ~1 degree/min (i.e., natural cooling process without using any coolants)). The temperature window for obtaining the highest feature contrast was observed to be always between 80−90 °C. In addition, we also found that the imprinting results are quiet independent of the gauge pressure in the range of 1.4−5.5 MPa. Therefore, we believe that such an optimum temperature window is attributed to the property of SubPc-A but not to the imprinting system.

As a comparison, a 200 nm period line/spacing Si template (from Nanonex Corporation, depth = 100 nm) was used to imprint SubPc-A with the same im-

print conditions. The dependence of the final feature depth (measured by AFM) on the imprinting temperature (Figure 4b) is very similar to the result shown in Figure 4a and also exhibits the best imprint temperature window at 80−90 °C. Imprinting by both templates results in a final equilibrium aspect ratio of imprinted features in SubPc-A that is shallower than that of the template features and exhibits a strong dependence on the imprinting temperature.

We attribute the postimprint feature relaxation to surface diffusion, driven by a reduction in surface energy; surface diffusion is pronounced in such small-molecular-weight organic compounds.[8,9] The improvement in feature stability between 80−90 °C is related to a change in the crystallinity as demonstrated by X-ray diffraction (XRD) data (Figure 5). XRD spectra of SubPc-A samples imprinted at various temperatures were measured and are plotted in Figure 5a. It is shown that the SubPc-A samples imprinted at $T < 70$ °C do not exhibit any noticeable features, indicating a low degree of crystallization. However, the XRD spectra of samples imprinted at 80−90 °C display very clear peaks associated with molecular stacking (or crystallization). This temperature range exactly coincides with the imprint temperatures leading to the highest feature contrast (see Figure 4). As the temperature is increased above 90 °C, the degree of crystallinity in the imprinted samples decreases and is almost undetectable when $T > 110$ °C. Correspondingly, the imprint at such relatively higher temperatures creates a relatively poor feature contrast (see Figure 4).

A powder diffractogram was simulated using the single crystal structure for SubPc-A, and a 3D representation of the crystal structure is illustrated in Figure 5b. The single crystal SubPc-A has a monoclinic crystal structure characterized with *P*2(1)/*c* space group. On the basis of the simulation in combination with previously reported XRD data of other SubPcs, the observed peaks in Figure 5a are indexed as (002) and (003).[13] The absence of other XRD peaks in imprinted SubPc-A samples indicates that SubPc molecules, subject to an imprinting pressure at specific temperatures, exhibit a preferential alignment of the molecular crystals with the (001) orientation that is perpendicular to the substrate.

Thus, the final aspect ratio of imprinted features in SubPc-A is highly correlated with the degree of crystallization and both are dependent on imprinting temperature. In addition, nanoimprint-induced molecular stacking may partially stabilize the imprinted features in SubPc-A, as is seen in models of surface diffusion of crystalline films on substrates.[12] This is investigated further in the following section.

To extrapolate the relationship between nanoimprint-induced molecular stacking and final feature aspect ratio, we consider how the imprinted features in the film morphology affect the free energy.

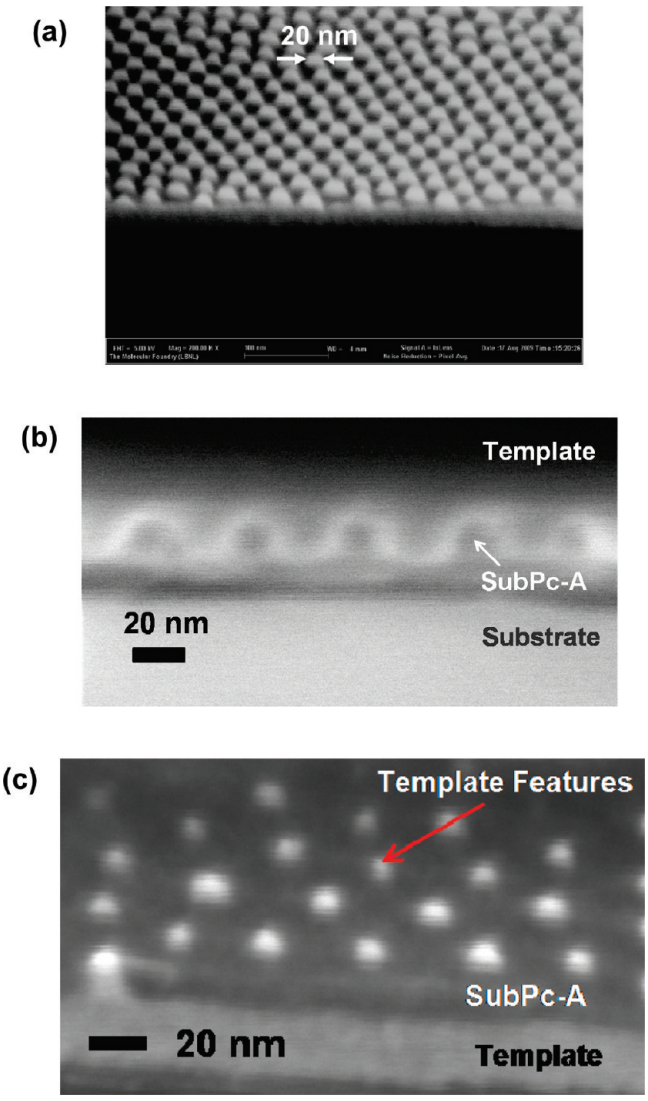

Figure 2. (a) The tilted SEM image of a SiO_2/Si nanoimprint template bearing hexagonally arranged posts with a diameter of 20 nm and a feature height of ~22 nm, which were fabricated through block-copolymer self-assembly followed with plasma etching. (b) The cross-sectional SEM image displaying a representative imprinting process (imprinting pressure: 3.4 MPa, imprinting temperature: 120 °C), which was achieved by mechanically cutting template/SubPc-A/substrate together before template separation. (c) The tilted SEM image showing that the SubPc-A layer is fully conformal to the template features without forming any visible voids. Here, the flat substrate was intentionally removed from the SubPc-A layer, and the residual layer in SubPc-A was etched away to partially expose the template features.

When an imprinting template is pressed into an as-spun SubPc-A layer, the densely arranged template features modulate the SubPc-A surface and significantly increase the surface energy of the film. In addition, a gradient in surface chemical potential is created wherein molecules are driven to diffuse from crests to troughs.[12,17] If the surface energy density $\gamma(\theta)$ is isotropic or weakly anisotropic with respect to surface orientation (case for amorphous solids), the free energy is minimized by lowering the total surface area. Hence, the imprinted SubPc-A surface relaxes to flat morphology. However, in the case of strong anisotropy (i.e., mo-

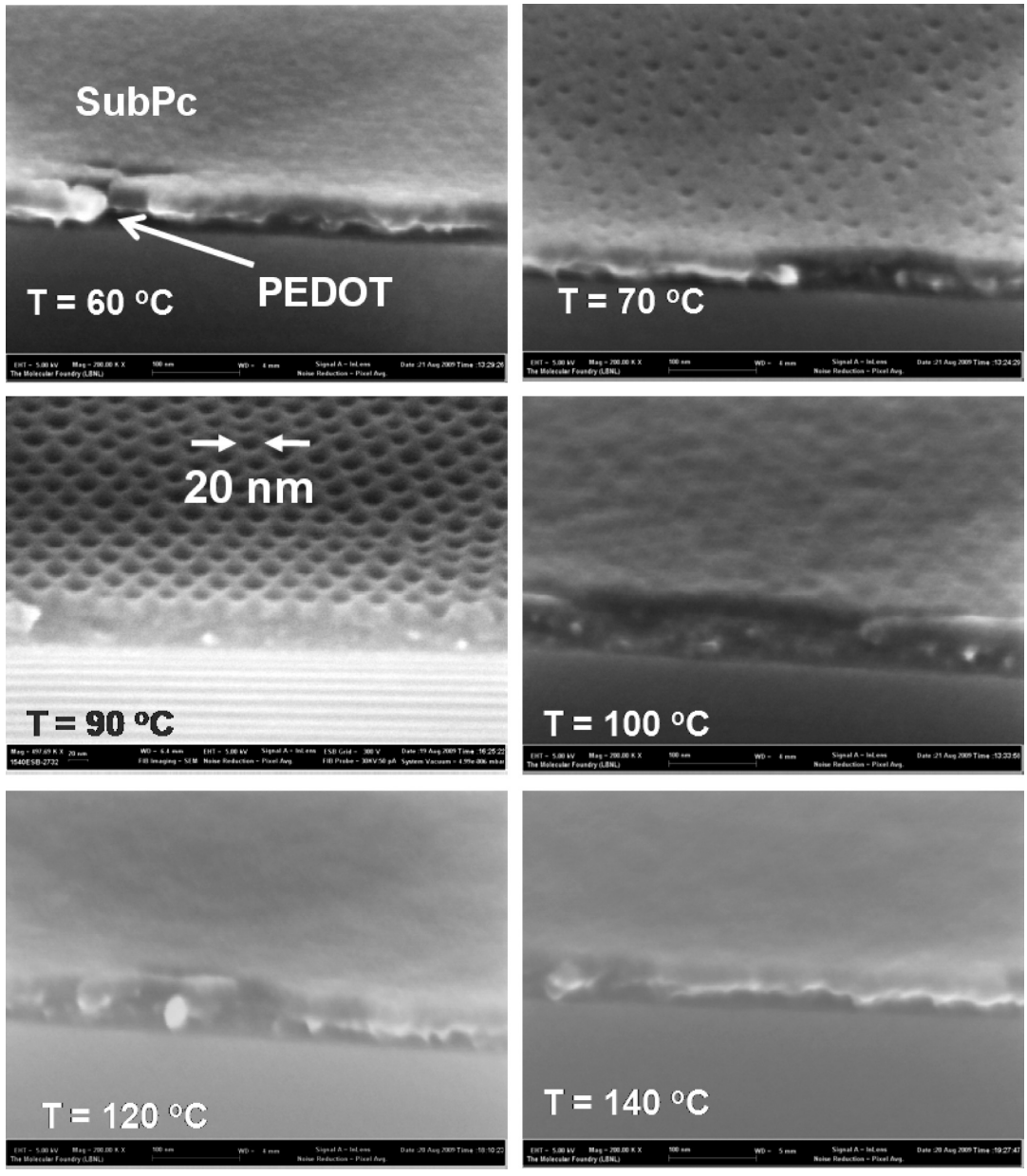

Figure 3. Tilted SEM images of the SubPc-A layers imprinted at various temperatures (60−140 °C), using the template shown in Figure 2b. For all the samples, the imprinting pressure is 3.4 MPa, the process time is 10 min, and the template was separated from the SubPc layers always at the room temperature (20 °C).

lecular crystals), the total energy may be minimized by faceting such that the imprinted features will maintain a finite aspect ratio. We have created a simple model which minimizes the total energy of the surface to understand the final feature aspect ratio as a function of the imprint pattern and surface energy anisotropy (which in turn is dependent on the degree of crystallinity and imprint temperature).

First, we assume that the surface energy density γ of imprinted SubPc-A samples depends on the orientation angle, θ, of a vicinal surface relative to (001) vector but is independent of the orientation angle in the substrate surface ($X-Y$ plane). This assumption is consistent with the XRD spectra (Figure 5a) that shows the nanoimprint-induced molecular stacking is preferentially aligned toward the (001) direction perpendicular to the substrate surface, whereas the stacking along other orientations is much less dominant. Following Bonzel *et al*,[18] we express the anisotropy of $\gamma(\theta)$ over a crystallographic zone with respect to the (001) surface as eq 1.

$$\gamma(\theta) = \gamma_0\left(1 + \varepsilon \sin\left(\frac{\pi}{2}\frac{\theta}{\theta_0}\right)\right) \quad (1)$$

Here ε is the degree of anisotropy, which is dependent on the degree of crystallization, θ_0 is the orientation angle where $\gamma(\theta)$ is maximum (usually associated with the high-index crystalline surfaces), and γ_0 is the surface energy of the (001) crystalline surface. The dependence of $\gamma(\theta)$ on θ is sketched in Figure 6a.

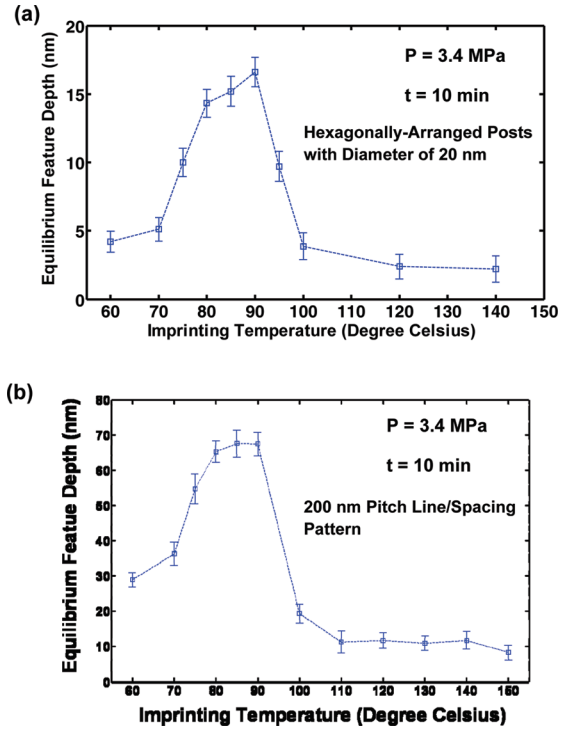

Figure 4. (a) For the imprinting results exhibited in Figure 3, the feature depths were measured by using cross-sectional SEM in combination with AFM and plotted as a function of imprinting temperatures. (b) Another template with 200 nm period line/spacing features (height = 100 nm) was used to imprint SubPc-A under the same condition, and a very similar dependence of the final feature depth (measured by AFM) on the imprinting temperature was obtained.

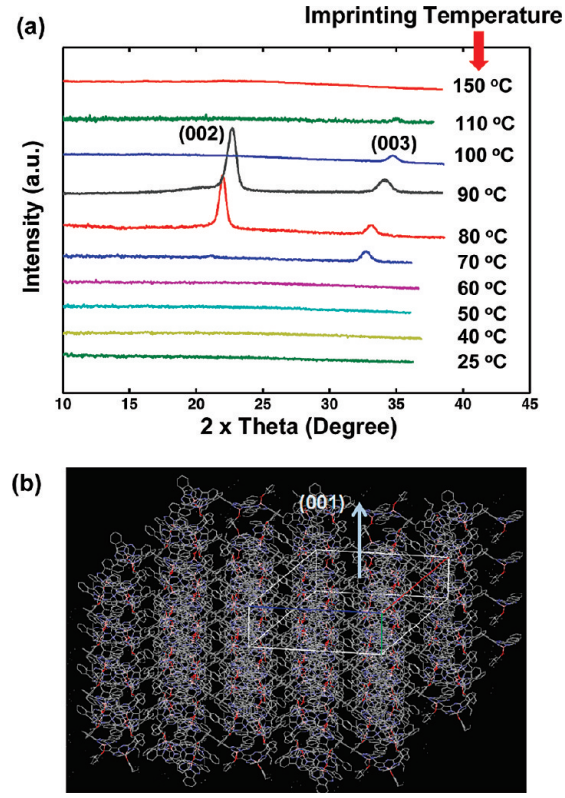

Figure 5. (a) XRD spectra of SubPc samples imprinted at various temperatures (i.e., the same batch of samples exhibited in Figure 3). (b) 3D representation of the single crystal structure of SubPc-A obtained *via* a powder diffractogram.

We use simple mathematical functions to mimic imprinted profiles of hexagonally arranged holes (eq 2, Figure 6b) and one-dimensional (1D) gratings (eq 3, Figure 6c):

$$h(x,y) = h_0 + d\left|\cos\left(\frac{\pi}{\lambda}x\right)\cos\left(\frac{\pi}{\lambda}\left(\frac{1}{2}x + \frac{\sqrt{3}}{2}y\right)\right)\right| \quad (2)$$

$$h(x) = h_0 + \frac{d}{2}\cos\left(\frac{2\pi}{\lambda}x\right) \quad (3)$$

in which h_0 is the initial thickness of as-spun SubPc-A layers; d is the feature depth (or amplitude); and λ is the feature period.

The total free energy G of a given imprinted surface area S can be calculated by eq 4 where r is the radius of surface curvature, a is the crystal lattice constant (XRD data measure $a \approx 0.77$ nm), γ_2 is a constant parameter in the order of $\gamma_0 a^2$, $\vec{n}$ is the outward surface-normal unit vector, and dS_n is the differential surface element, as illustrated in Figure 6c.[19]

$$G \propto \iint_S \left(\gamma + \frac{\gamma_2}{r^2}\right) dS_{\vec{n}} \qquad \gamma_2 \approx O(\gamma_0 a^2) \quad (4)$$

Given a set of parameters of λ, ε, and θ_0, the total film free energy G is calculated and plotted as the function of nominal feature depth, d, to evaluate the final equilibrium profile of the imprinted nanostructures (here, we assume $\gamma_0 = 1$). In terms of thermodynamic stability, the equilibrium depth (or height) of imprinted periodic features can be determined by locating the local minimum point on $G-d$ curves. Figure 7a plots the simulated $G-d$ curves for various values of ε ($\lambda = 33$ nm, $\theta_0 = 15°$). For a zero or relatively weak anisotropy of surface energy ($\varepsilon < 0.1$), the total film free energy G is monotonic with respect to the nominal imprint depth d, and no local minimum point can be located on the $G-d$ curve. This is the case for imprint into an amorphous material layer with very weak crystallinity. In this case, there is a driving force making the imprinted surface relax to the flat surface ($d \approx 0$), resulting in a significant loss of feature contrast. For the case of strong anisotropy (or high crystallinity $\varepsilon > 0.1$), a local minimum point with $d > 0$ is found on $G-d$ curves. Our model indicates that as the degree of anisotropy (or molecular stacking) increases, the local minimum is pushed toward the higher aspect ratio of the imprinted features. This is consistent with our experimental results (Figure 4 and Figure 5).

Owing to the lack of measured values of ε, and θ_0 for SubPc-A, it is difficult to directly compare model calculation results with experimental data. However, our simulation indicates that for any values of ε and θ_0, the final equilibrium feature depth (or height) is linearly proportional to the feature period, as shown in Figure

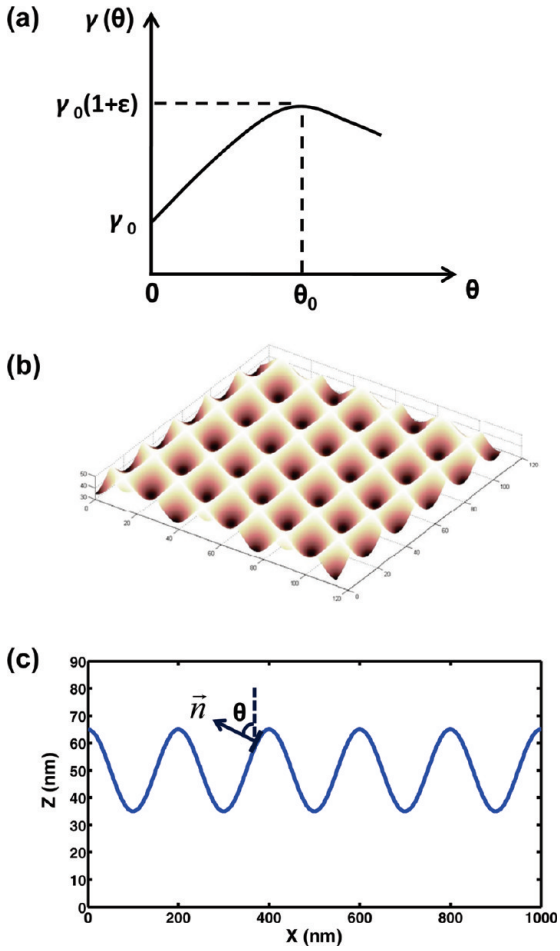

Figure 6. (a) Sketch of the surface energy $\gamma(\theta)$ of imprinted SubPc surface as a function of the orientation angle θ of a vicinal surface relative to (001) vector. Panels b and c are simple mathematical functions for mimicking imprinted profiles of hexagonally arranged holes and one-dimensional (1D) gratings, respectively.

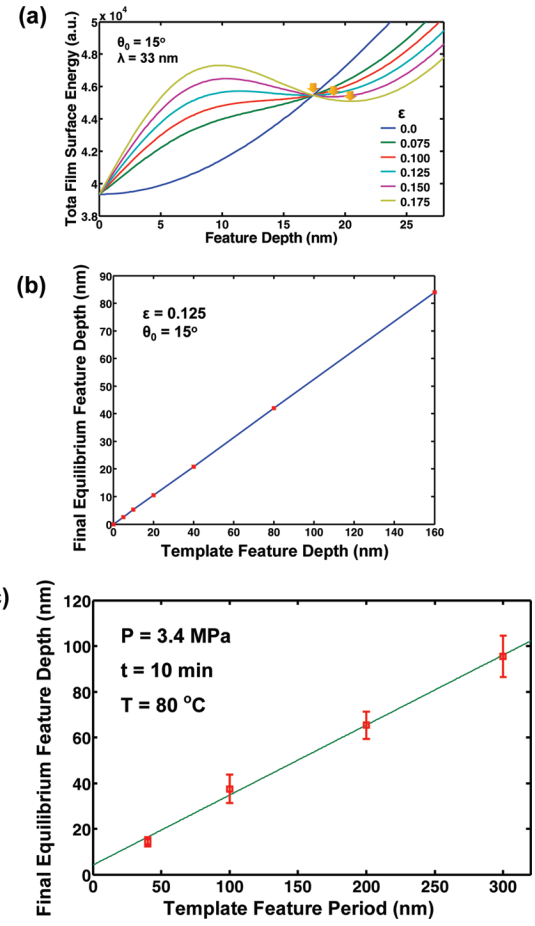

Figure 7. (a) Simulated total film free energy G as a function of nominal feature depth (or height) d for various values of degree of anisotropy ε under fixed feature period $\lambda = 33$ nm and $\theta_0 = 15°$. (b) Simulated final feature depth *versus* feature period ($\varepsilon = 0.125$, $\theta_0 = 15°$). (c) Experimentally measured final feature depth d as a function of feature period ($\lambda = 40$, 100, 200, 300 nm).

7b which displays the simulated final feature depth *versus* feature period ($\varepsilon = 0.125$, $\theta_0 = 15°$). In other words, the quasi-equilibrium feature aspect ratio (depth/half period) is primarily a function of the material crystallinity (ε and θ_0). To verify this predicted linearity, we imprinted SubPc-A using templates with various feature periods, which include 40 nm period pillars (Figure 2a) and line/spacing patterns with periods of 100, 200, and 300 nm (Figure S1 in the Supporting Information file shows the SEM images of all line/spacing templates). All templates have a feature aspect ratio (height/width) of ~1. The imprinting was performed at 80 °C under a gauge pressure of 3.4 MPa for 10 min. Figure S1d in the Supporting Information shows the tiled cross-sectional SEM image of SubPc-A imprinted by a 300 nm pitch template. The imprinted feature exhibits a cosine-like profile and a reduced aspect ratio in comparison to that of the template feature. This is attributed to the surface diffusion that can round off any sharp corners in the nanopatterns and reduce the feature contrast. Figure S2 in the Supporting Information file shows the atomic force micrographs (AFMs) of SubPc-A imprinted with various feature periods. The final feature depth d was measured from the AFM scanlines (peak-to-valley depth indicated by the arrows in Figure S2a). Figure 7c shows measured final feature depth d as a function of feature period λ. As expected by the simulation, d is linearly dependent on λ. This experimental result strongly supports our model of feature stabilization and relaxation in imprinted SubPc-A, which depends on the relationship between nanoimprint-induced crystallization and total surface energy. In our current calculation model, we did not take account into the effect of the stress in the film, which may play an important role in the deep imprinting (high-aspect case). Such residual stress in the imprinted materials may also contribute to the feature stabilization and will be further studied in our future work.

CONCLUSION

Thermal nanoimprint was studied as a lithographic tool for patterning SubPc-A, an attractive solution-processable small-molecular weight OPV material. The imprinted features quickly relax after template separa-

tion *via* surface diffusion. A suitable feature contrast was found within a very specific temperature window of 80−90 °C for the given imprinting pressure and time even as template feature size was varied. The final feature aspect ratio is highly correlated to the degree of molecular stacking which was also found to be within the 80−90 °C window. A model was used to simulate the key factors affecting the final feature contrast. These key factors include surface energy anisotropy, crystallinity, and feature period. The simulation and experimental results are in excellent agreement and show that surface energy anisotropy induced by the crystallinity creates a local minimum in the free energy when the surface remains modulated after imprint. However, amorphous films will minimize the free energy by relaxing to a flat, unmodulated surface. The analysis presented here can be generalized for other materials and serves as an important guideline for optimizing the nanopatterning of small-molecular weight organic compounds for photovoltaic applications. The performance of these nanoimprinted SubPc-A films as donor layers for organic photovoltaics is under investigation, and the results will be reported in the near future.

METHODS AND MATERIALS

The nanoimprint was performed in 2-allylphenoxy-(subphthalocyaninato) boron(III) (SubPc-A) (see Figure 1 for (a) chemical structure (b) 3D representation of molecular structure). The synthesis process and characterization of SubPc-A has been reported in previous publications.[14] Single crystals of SubPc-A were grown by slow diffusion of hexane into dichloromethane solutions. All measurements were made on a Bruker SMART 1000 CCD area detector with graphite monochromated Mo K (λ = 0.71073 Å) radiation at UC Berkeley College of Chemistry X-ray crystallography facility. The structure was solved by direct methods (SHELXS-97).

Here, the thin films of SubPc-A of 20−100 nm thick were prepared *via* the spin-coating of chlorobenzene solutions on blank silicon wafers. The higher resolution silicon imprint templates were patterned using block-copolymer self-assembly followed with plasma etching.[20,21] Figure 2a shows the tilted scanning electron micrograph (SEM) of a nanoimprint template bearing hexagonally arranged posts with a diameter of 20 nm and single-crystal domain size of hundreds of nanometers. The template surface was treated with a mold-release agent (MRA) for easy template removal without material peel-off. The 200 nm pitch line/spacing template was bought from Nanonex Corporation; 100 and 300 nm pitch line/spacing templates were patterned with electron beam lithography followed with reactive ion etching. All templates were cut into 1.25 cm ×1.25 cm size in order to fit the size of the substrate. Figure S1 in the Supporting Information file displays the SEM images of all line/spacing templates.

The thermal nanoimprint was performed on a Lawrence Berkeley National Laboratory homemade nanoimprinter with controllable thermal cycle. During the thermal nanoimprint cycle, the template and the substrate are first pressed together by using a pair of parallel metal plates, which can generate a gauge pressure ranging from 0.7 to 7.0 MPa. Next, two resistive heaters built inside the parallel plates heat the samples, and the temperature ramps up from room temperature to the designated temperature in about 1 min. Then the imprinting temperature is stabilized at the designated temperature for 10 min. Afterward the heaters are turned off, and the sample temperature ramps down. During the cooling process, the imprinting pressure remains until the sample cools to the room temperature. Finally, the template is separated from the substrate.

The imprinted SubPc-A nanostructures were characterized by cross-sectional SEM, atomic-force microscopy (Veeco Caliber SPM−AFM), and X-ray diffraction (XRD) spectroscopy (Bruker AXS D8 Discover GADDS XRD diffractometer, λ = 1.54178 Å).

Acknowledgment. This work was supported by the Director, Office of Science, Office of Basic Energy Sciences, Materials Sciences and Engineering Division, of the U.S. Department of Energy under Contract No. DE-AC02-05CH11231. The authors would like to thank Antonio G. DiPasquale and Clayton Mauldin at UC Berkeley for help with single crystallography and Prof. J. Bokor for helpful discussion.

Supporting Information Available: (Figure S1) SEM images of line/spacing templates with feature periods of (a) 100, (b) 200, and (c) 300 nm. Figure S1d shows the tiled cross-sectional SEM image of a representative SubPc-A layer imprinted by using the line/spacing template; (Figure S2) the AFM images of imprinted SubPc-A layers with feature periods of (a) 100, (b) 200, and (c) 300 nm. The corresponding insets show the scanlines corresponding to the locations designated by the green lines in the AFM images. This material is available free of charge *via* the Internet at http://pubs.acs.org.

REFERENCES AND NOTES

1. Tang, C. W. 2-Layer Organic Photovoltaic Cell. *Appl. Phys. Lett.* **1986**, *48*, 183–185.
2. Yu, G.; Gao, J.; Hummelen, J. C.; Wudl, F.; Heeger, A. J. Polymer Photovoltaic Cells—Enhanced Efficiencies *via* A Network of Internal Donor−Acceptor Heterojunctions. *Science* **1995**, *270*, 1789–1791.
3. Rand, B. P.; Burk, D. P.; Forrest, S. R. Offset Energies at Organic Semiconductor Heterojunctions and Their Influence on the Open-Circuit Voltage of Thin-Film Solar Cells. *Phys. Rev. B* **2007**, *75*, 11.
4. Chou, S. Y.; Krauss, P. R.; Renstrom, P. J. Imprint of Sub-25 nm Vias and Trenches in Polymers. *Appl. Phys. Lett.* **1995**, *67*, 3114–3116.
5. Kim, M. S.; Kim, J. S.; Cho, J. C.; Shtein, M.; Guo, L. J.; Kim, J. Flexible Conjugated Polymer Photovoltaic Cells with Controlled Heterojunctions Fabricated Using Nanoimprint Lithography. *Appl. Phys. Lett.* **2007**, *90*, 3.
6. Cheyns, D.; Vasseur, K.; Rolin, C.; Genoe, J.; Poortmans, J.; Heremans, P. Nanoimprinted Semiconducting Polymer Films with 50 nm Features and Their Application to Organic Heterojunction Solar Cells. *Nanotechnology* **2008**, *19*, 6.
7. Peumans, P.; Yakimov, A.; Forrest, S. R. Small Molecular Weight Organic Thin-Film Photodetectors and Solar Cells. *J. Appl. Phys.* **2003**, *93*, 3693–3723; erratum: *J. Appl. Phys.* **2005**, *95*, 2938.
8. Michel, B.; Bernard, A.; Bietsch, A.; Delamarche, E.; Geissler, M.; Juncker, D.; Kind, H.; Renault, J. P.; Rothuizen, H.; Schmid, H.; Schmidt-Winkel, P.; Stutz, R.; Wolf, H. Printing Meets Lithography: Soft Approaches to High-Resolution Patterning. *Chimia* **2002**, *56*, 527–542.
9. Truskett, V. N.; Watts, M. P. C. Trends in Imprint Lithography for Biological Applications. *Trends Biotechnol.* **2006**, *24*, 312–317.
10. Guo, L. J. Nanoimprint Lithography: Methods and Material Requirements. *Adv. Mater.* **2007**, *19*, 495–513.
11. Khenner, M. Tailoring of Crystal Surface Morphology by Induced Spatiotemporal Oscillations of Temperature. *Phys. Rev. E* **2007**, *75*, 14.
12. Khenner, M. Dewetting of an Ultrathin Solid Film on a Lattice-Matched or Amorphous Substrate. *Phys. Rev. B* **2008**, *77*, 7.

13. Claessens, C. G.; Gonzalez-Rodriguez, D.; Torres, T. Subphthalocyanines: Singular Nonplanar Aromatic Compounds-Synthesis, Reactivity, and Physical Properties. *Chem. Rev.* **2002**, *102*, 835–853.
14. Ma, B.; Miyamoto, Y.; Woob, C. H.; Fréchet, J. M. J.; Zhang, F.; Liu, Y. Solution Processable Boron Subphthalocyanine Derivatives as Active Materials for Organic Photovoltaics. *Proc. SPIE* **2009**, *7416*, 74161E.
15. Ma, B.; Woob, C. H.; Miyamoto, Y.; Fréchet, J. M. J. Solution Processing of a Small Molecule, Subnaphthalocyanine, for Efficient Organic Photovoltaic Cells. *Chem. Mater.* **2009**, *21*, 1413–1417.
16. Ge, H. X.; Wu, W.; Li, Z. Y.; Jung, G. Y.; Olynick, D.; Chen, Y. F.; Liddle, J. A.; Wang, S. Y.; Williams, R. S. Cross-linked polymer replica of a nanoimprint mold at 30 nm half-pitch. *Nano Lett.* **2005**, *5*, 179–182.
17. Burger, M. Surface Diffusion Including Adatoms. *Commun. Math. Sci.* **2006**, *4*, 1–51.
18. Bonzel, H. P.; Preuss, E. Morphology of Periodic Surface Profiles Below The Roughening Temperature—Aspects of Continuum Theory. *Surf. Sci.* **1995**, *336*, 209–224.
19. Herring, C. Some Theorems on The Free Energies of Crystal Surfaces. *Phys. Rev.* **1951**, *82*, 87–93.
20. Jung, Y. S.; Ross, C. A. Orientation-controlled Self-Assembled Nanolithography Using a Polystyrene-Polydimethylsiloxane Block Copolymer. *Nano Lett.* **2007**, *7*, 2046–2050.
21. Park, H. J.; Kang, M. G.; Guo, L. J. Large Area High Density Sub-20 nm SiO_2 Nanostructures Fabricated by Block Copolymer Template for Nanoimprint Lithography. *ACS Nano* **2009**, *3*, 2601–2608.